PHYSICAL REVIEW A **76**, 063620 (2007)

Excitation spectrum of bosons in a finite one-dimensional circular waveguide via the Bethe ansatz

Andrew G. Sykes,* Peter D. Drummond, and Matthew J. Davis
ARC Centre of Excellence for Quantum-Atom Optics, School of Physical Sciences, University of Queensland, Brisbane, Queensland 4072, Australia

(Received 15 July 2007; published 27 December 2007)

The exactly solvable Lieb-Liniger model of interacting bosons in one dimension has attracted renewed interest as current experiments with ultracold atoms begin to probe this regime. Here we numerically solve the equations arising from the Bethe ansatz solution for the exact many-body wave function in a finite-size system of up to 20 particles for attractive interactions. We discuss the features of the solutions, and how they deviate from the well-known string solutions [Thacker, Rev. Mod. Phys. **53**, 253 (1981)] at finite densities. We present excited state string solutions in the limit of strong interactions and discuss their physical interpretation, as well as the characteristics of the quantum phase transition that occurs as a function of interaction strength in the mean-field limit. Finally we compare our results to those of exact diagonalization of the many-body Hamiltonian in a truncated basis. We also present excited state solutions and the excitation spectrum for the repulsive one-dimensional Bose gas on a ring.

DOI: 10.1103/PhysRevA.76.063620 PACS number(s): 03.75.Hh, 03.65.Ge

I. INTRODUCTION

Physics in low-dimensional systems has long provided a rich source of fascinating and often unexpected phenomena. With the steady progress of experimental methods in ultracold gases, effective one-dimensional systems are beginning to be realized in the laboratory [1–10]. The integrability of certain many-body problems in one dimension [11,12] provides an opportunity to reliably examine many-body quantum physics beyond mean-field theory. It is becoming clear that many condensed matter theories of phase transitions and collective excitations depend on the number of degrees of freedom within the system [13,14].

In this paper we focus on a system of identical bosons tightly confined in a ring trap such that the system can be considered to be purely one dimensional (but with three-dimensional scattering). We are primarily interested in obtaining the excitation spectrum of the system. The motivation for this work was provided by the prediction of a quantum phase transition in the regime of attractive interactions. As the interaction strength for a fixed number of particles becomes more negative, zero-temperature quantum fluctuations eventually cause the gas to form a solitonlike localized state [20,21]. Quantum solitons in one-dimensional (1D) Bose gases were first predicted and observed with photons in optical fibers [15,16], and more recently solitonlike behavior has been observed in systems of massive particles with attractive interactions in quasi-1D [17,18] and 3D geometries [19].

The quantum phase transition in the 1D toroidal geometry was initially identified using a mean-field approach by Kavoulakis [20] and Kanamoto *et al.* [21,22]. Further work by Kanamoto *et al.* has taken a quantum many-body approach using exact diagonalization by truncating the Hilbert space to three (or five) single-particle states for up to 200 atoms [23,24]. They found a number of interesting physical features in the region of the phase transition, in particular, evidence of symmetry breaking as the difference in energy between the ground and first excited states tended to zero and scaled as $N^{-1/2}$.

While the results obtained by Kanamoto *et al.* [23,24] remain qualitatively correct at low temperature and weak interactions, the Bethe ansatz provides us with an exact solution for all excited states of the system at all values of interaction strength. The ground state quasimomenta and energy for the one-dimensional Bose gas have previously been calculated using the Bethe ansatz for both periodic and hard-wall boundary conditions by Sakmann *et al.* [25] and Hao *et al.* [58], respectively. However, we emphasize that for experimentally realistic temperatures for this system excited states will be involved in both the static and dynamic properties of the system. In this paper we extend the work of Sakmann *et al.* [25] to calculate the low-lying excitation spectrum of the finite one-dimensional Bose gas on a ring as a function of interaction strength for up to $N=20$ particles. This is a nontrivial result due to the complicated behavior of the quasimomenta in the complex plane in the attractive case (see Sec. III A). To the best of our knowledge, this work is the first example of calculations made on excited states of this system (with more than three particles) without any truncation of the Hilbert space and without restricting oneself to the limiting *string* solutions.

The string solutions arise in the case where the interatomic interactions are sufficiently attractive, or alternatively in the zero-density limit. The problem reduces to one solved by McGuire [12] and elaborated upon in Refs. [26,27]. The point of interest in our numerical solutions is the deviations of the quasimomenta from these previously known solutions. Our present work extends our understanding of quantum solitons from the large boson numbers in optical fibers toward the much smaller numbers possible in atomic systems.

Related work has been performed by Oelkers and Links [28], who concentrate on a toroidal lattice governed by the

*sykes@physics.uq.edu.au

Bose-Hubbard Hamiltonian with periodic boundary conditions. Physically one expects the results of their calculations to tend toward those of the continuum as the number of lattice sites increases. The Bose-Hubbard Hamiltonian is, however, nonintegrable, and it has been shown by Seel *et al.* [29] that the spin-1/2 *XXZ* Heisenberg chain (which is integrable) maps onto the 1D Bose gas model in the continuum limit. Other examples of lattice Hamiltonians that have the 1D Bose gas in the continuum limit can be found in [30–32].

The structure of this paper is as follows. In Sec. II we review the work of Lieb and Liniger [11] in order to correctly pose the problem. In Sec. III A we discuss our method of solution and present the results, while also discussing its connection to earlier work by McGuire [12]. In Sec. III B we present the excitation spectrum of the system obtained from our calculations, and in Sec. III C we show a comparison of our work to that of the truncated Hilbert space approach of Refs. [23,24]. Finally we calculate the excitation spectrum for the repulsive case in Sec. IV, before concluding in Sec. V.

II. THE MODEL

We consider a system of N bosons of mass m confined in a toroidal trap of radius R. It is possible to define a *local* set of Cartesian coordinates such that the z axis runs tangential to ring. We assume sufficiently tight harmonic confinement in the xy dimensions transverse to the ring such that they are frozen out. Defining the transverse oscillator length $x_0 = \sqrt{\hbar/(m\omega_x)} \ll R$, as long as the scattering length a representing the strength of two-body interactions satisfies $|a| \ll x_0$, we can integrate out the transverse dimensions to give us an effective 1D system with periodic boundary conditions. The dimensionless Hamiltonian in first quantization is then

$$H = \sum_{j=1}^{N} -\frac{\partial^2}{\partial \theta_j^2} + 2c \sum_{i<j} \delta(\theta_i - \theta_j), \tag{1}$$

where length is measured in units of R, energy is measured in units of $\hbar^2/2mR^2$, and θ_i is the angular coordinate of the ith particle. The parameter c is related to the s-wave scattering length by

$$c = \frac{\hbar^2}{m}\frac{a}{x_0^2}, \tag{2}$$

and quantifies the strength of the two-body interactions. If $c<0$ we have an attractive gas while $c>0$ describes a repulsive gas.

Some interesting work has recently been done by Parola *et al.* [33,34] on the quasi-one-dimensional limit which indicated a transverse collapse (in addition to the angular collapse) at a certain critical interaction strength. In this work they took into closer consideration the effects of the two excluded dimensions. Current experimental realizations of such ring traps [35] are still far from the quasi-1D regime [36–40].

Given the Hamiltonian (1), Schrödinger's equation is

$$H\psi_n(\theta_1, \ldots, \theta_N) = E_n \psi_n(\theta_1, \ldots, \theta_N), \tag{3}$$

where n is the label for different eigenstates. Equation (3) can be solved exactly via the Bethe ansatz [11]. Due to the symmetry under permutation of particle coordinates, the region over which we need to integrate Eq. (3) can be restricted to $0 \le \theta_1 \le \cdots \le \theta_N \le 2\pi$. Lieb and Liniger noted that in this region the δ function vanishes everywhere except along the boundaries where $\theta_i = \theta_{i+1}$; hence the problem could be cast in a different manner by writing the interactions as a *boundary condition* on the restricted region rather than an explicit term in the Hamiltonian [11]. The new problem was to find the appropriate solution to

$$-\sum_{j=1}^{N} \frac{\partial^2 \psi_n}{\partial \theta_j^2} = E_n \psi_n \quad \text{in the restricted region,} \tag{4}$$

$$\left(\frac{\partial}{\partial \theta_{j+1}} - \frac{\partial}{\partial \theta_j}\right)\psi_n \Big|_{\theta_{j+1}=\theta_j} = c\psi_n|_{\theta_{j+1}=\theta_j}, \tag{5}$$

where Eq. (5) is the previously mentioned boundary condition arising from the interaction. Furthermore, the boundary conditions pertaining to the ring geometry of the system, i.e., $\psi_n(\ldots, \theta_i, \ldots) = \psi_n(\ldots, \theta_i + 2\pi, \ldots)$, must also be recast onto the new region, that is,

$$\psi_n(0, \theta_2, \ldots, \theta_N) = \psi_n(\theta_2, \ldots, \theta_N, 2\pi), \tag{6a}$$

$$\frac{\partial}{\partial \theta}\psi_n(\theta, \theta_2, \ldots, \theta_N)|_{\theta=0} = \frac{\partial}{\partial \theta}\psi_n(\theta_2, \ldots, \theta_N, \theta)|_{\theta=2\pi}. \tag{6b}$$

The Bethe ansatz is employed as a means of integrating Eq. (4). The (unnormalized) wave function in the restricted region is given the form

$$\psi_n(\theta_1, \ldots, \theta_N) = \sum_{\{Q\}} A_Q^{(n)} \exp\left(i \sum k_{Q(j)}^{(n)} \theta_j\right), \tag{7}$$

where Q is some permutation of the integers $1, 2, \ldots, N$, $Q(j)$ is the jth element in Q, and the sum runs over all the $N!$ distinct permutations of Q. Equation (7) is one form of the Bethe ansatz and was originally used as a means of integrating spin chain Hamiltonians [41]. The coefficients of each permutation, $A_Q^{(n)}$, can be determined (up to some arbitrary phase) by the interaction boundary condition Eq. (5). We choose the convention $A_{12,\ldots,N}^{(n)} \equiv 1$, and for any other permutation Q, $A_Q^{(n)}$ is found by constructing Q out of $1, 2, \ldots, N$ by transposing adjacent elements. Then $A_Q^{(n)}$ is a product of the terms

$$-\frac{k_{Q(a)}^{(n)} - k_{Q(b)}^{(n)} + ic}{k_{Q(a)}^{(n)} - k_{Q(b)}^{(n)} - ic},$$

where $Q(a)$ and $Q(b)$ are the adjacent elements being transposed, with $Q(a)$ to the left of $Q(b)$ *before* the transposition.

The scalar quantities $k_1^{(n)}, \ldots, k_N^{(n)}$, known as the *quasimomenta* (and sometimes the rapidities), are determined by the ring geometry of the system, i.e., by the boundary conditions in Eqs. (6a) and (6b). These quasimomenta furnish important quantities for the system such as the energy eigenvalues and the total momentum; however, it should be stressed that (other than the case of no interactions $c=0$) the individual

quasimomenta do not have a direct relationship to the single-particle momentum states. The latter must be obtained from the single-particle reduced density operator, which in principle can be obtained from the many-body wave function.

Substitution of Eq. (7) into the boundary conditions (6a) and (6b) yield the following set of N simultaneous equations to determine the quasimomenta as functions of c:

$$(-1)^{N-1}e^{-i2\pi k_j} = \prod_{s=1}^{N} \frac{k_j - k_s + ic}{k_j - k_s - ic}, \quad j = 1, \ldots, N. \tag{8}$$

The purpose of this work is to explore solutions of these equations to reveal key features of the system such as the excitation spectrum of the gas as a function of the interaction strength. Analytical solutions of Eq. (8) have previously been found for up to three particles [42]; however, to our knowledge the only numerical calculations have been for the ground state energy [25]. Once Eqs. (8) have been solved it is true that, in principle at least, one has obtained all neccessary information to obtain the wave function for the system. However, in practice, even for a modest number of particles such as ten, the wave function itself will involve a summation over $10! \approx 4 \times 10^6$ terms, a somewhat cumbersome object. However, for certain physical quantities, simple analytical expressions involving only the quasimomenta can easily be derived; for instance, the energy of the nth eigenstate is given by

$$E_n = \sum_{j=1}^{N} k_j^{(n)2}, \tag{9}$$

and likewise the total momentum by

$$P_n = \sum_{j=1}^{N} k_j^{(n)}. \tag{10}$$

We will utilize Eq. (9) in Sec. III B to obtain the excitation spectrum.

III. ATTRACTIVE GAS: $c < 0$

The behavior of the Bose gas with attractive interactions has received far less scrutiny than its repulsive counterpart. Originally Lieb and Liniger did not consider this regime to be of physical relevance [11]; however, McGuire showed [12] that once an N-particle bound state has formed, the ground state energy of the system scales as

$$E_0 \propto -c^2 N(N^2 - 1). \tag{11}$$

This posed problems for the solution in the thermodynamic limit where $N \to \infty$, $R \to \infty$, and $N/R = \text{const}$. In contrast, for the repulsive case it is found that $E_0 \propto N \propto R$, and hence an expression for the energy density could be found [43–46]. However, E/R diverges in the attractive regime. It is perhaps worth noting that the limit of an extremely dilute gas is free from these divergences, provided one takes the limit as $N^3/R = \text{const}$. Another possibility is to consider the limit $R \to \infty$ while N remains constant [12,27,47,48].

As previously mentioned, the quantum phase transition to a solitonlike state provides added interest for the attractive gas. This transition spontaneously breaks the translational symmetry of the system even at zero temperature. We discuss this point further in Sec. III A and see how the eigenstates obtained from the Bethe ansatz maintain the translational symmetry of the Hamiltonian by forming a continuous superposition of localized states around the ring. We have included in Appendix B a simple derivation (following the work of Kavoulakis [20]) of the critical interaction strength ($C_0 = -\pi/2N$) at which the phase transition is predicted to occur.

The current work is restricted to relatively small numbers of particles compared to those considered in a mean-field analysis which typically takes $N \to \infty$ while keeping cN constant [20,21,57]. This is unavoidable due to the computational difficultly of simultaneously solving the N Bethe ansatz Eqs. (8). However, in this case, where an exact many-body solution exists, it useful to see the emergence of the mean-field physics as the numbers of particles are increased.

A. Quasimomenta

To find the quasimomenta $\{k_i\}$ that fully characterize the exact solution, we must numerically solve Eqs. (8), which for N particles gives N simultaneous nonlinear equations. The nature of most root-finding algorithms is such that it requires a reasonable initial guess for the location of the roots. We have developed a suitable procedure to solve these equations for a range of interaction strengths c starting from the known solutions for the ground and excited states at $c = 0$, which are given by all k_i being an integer.

To find the solution for nonzero c, we first choose a value for c close to zero, and use the ideal gas solution for the state we are interested in as the initial guess for the root-finding algorithm. We make use of the built-in root finder FSOLVE in the software package MATLAB on a standard desktop PC. By choosing a small enough c, the initial guess for the quasimomenta is close to the actual solution, and the root-finding algorithm converges relatively rapidly [49].

Once the first solution close to $c = 0$ is found, c is decreased in small increments Δc and an initial guess for the quasimomenta for the new value of c is based on a smooth extrapolation from the previous values. Typically the extrapolation is based only on the two previous values of c and is thus linear. Difficulties arise in this method when a particular quasimomentum at an interaction strength c differs greatly from that at $c + \Delta c$. This problem arises particularly when c is close to the critical interaction strength c_0 and we discuss how we deal with the problem below.

The actual size of Δc will be dependent on how large N is. The scaling behavior of the critical interaction strength varies as $C_0 \propto 1/N$ and we find that the efficiency of the algorithm is improved by using Δc as small as $10^{-3}/N$. It is possible to use a larger value of Δc, but we have found that smaller step sizes give better initial predictions for the roots for the next step and results in faster convergence of the root-finding algorithm.

We have not found it necessary to make use of high-precision arithmetic used by Sakmann *et al.* [25] in finding our solutions. In their work they make use of a particular

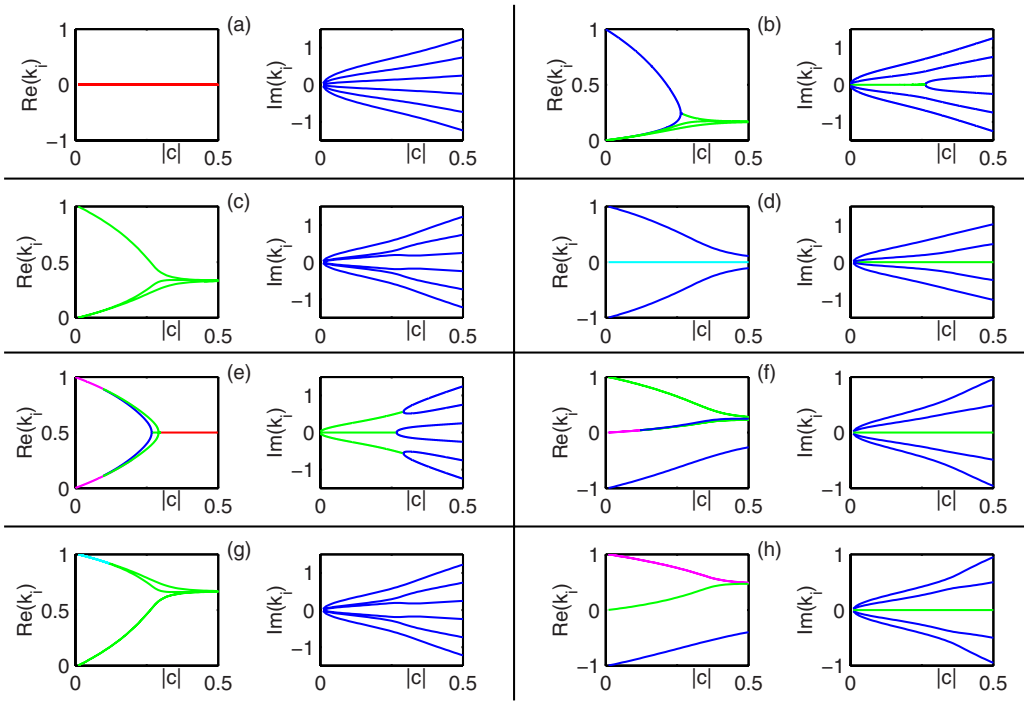

FIG. 1. (Color online) Behavior of the quasimomenta for $N=6$ particles as a function of the interaction strength $c<0$, for eight low-lying states, ordered via their energy at $c=0$. The single-particle momentum states (and their energies) at $c=0$ are (a) $\{0,0,0,0,0,0\}$ $(E=0)$, (b) $\{1,0,0,0,0,0\}$ $(E=1)$, (c) $\{1,1,0,0,0,0\}$ $(E=2)$, (d) $\{1,-1,0,0,0,0\}$ $(E=2)$, (e) $\{1,1,1,0,0,0\}$ $(E=3)$, (f) $\{1,1,-1,0,0,0\}$ $(E=3)$, (g) $\{1,1,1,1,0,0\}$ $(E=4)$, and (h) $\{1,1,1,-1,0,0\}$ $(E=4)$. All states shown have a total angular momentum that is either zero [(a) and (d)] or positive [(b), (c), (e), (f), (g), and (h)]—the latter set have a degenerate counterpart with a negative total angular momentum which can be found easily via the mapping $k_i \rightarrow -k_i$ for all i. The states plotted all have $|k_i| \leq 1$ for all i—states with quasimomenta such as $\{2,0,0,0,0,0\}$ at $c=0$, [which are degenerate with (g) and (h)] give rise to higher-energy states for $c<0$. On each graph there are six distinct lines for each particle; however, some of these overlap for large regions. To aid visualization the color of the lines indicates how many quasimomenta are overlapping. Blue indicates one root, green two, magenta three, cyan four, and red six.

transformation [see Eq. (33) in Ref. [25]] popularized in the seminal work of Lieb and Liniger [11]. The transformation simplifies the numerics in the repulsive case by *spreading* the transformed quasimomenta into numbers which can be easily distinguished by machine precision. The same is not true in the case of attractive interactions. As pointed out by Sakmann *et al.*, working with the transformed quasimomenta in the attractive case requires numerical precision of approximately 10^{-85}. In this work we solve Eqs. (8) directly. We set the tolerance of the FSOLVE algorithm to iterate until Eqs. (8) are solved such that the left hand side equals the right-hand side to an absolute accuracy of 10^{-10}. Once the value of $|c|$ has increased to the point that the quasimomenta are within 10^{-10} of the string solution, the algorithm terminates.

We present the results of these calculations in two different ways. Figures 1–3 show the continuous evolution of the real and imaginary parts of the quasimomenta for a number of excited states as c becomes more negative. Figure 1 shows eight low-lying excited states for $N=6$, whereas Figs. 2 and 3 show two representative excited states for $N=20$. Figures 4 and 5 show snapshots of the distribution of the quasimomenta in the complex plane for $N=20$. Our calculations elucidate the *deviations* from the string solutions at finite density [50].

We see from Figs. 1(b) and 1(e) that as the real parts of k_i and k_j become equal the imaginary parts *bifurcate*, and vice versa. These splittings of the quasimomenta provide additional challenges for the root-finding algorithm. Because the splitting often occurs sharply, the initial guess for the quasimomenta found from the previous value of c can be sufficiently inaccurate that the algorithm does not converge. Thus, if one finds that the root-finding algorithm is not converging at a particular value of c, then this could be an indication that two equal quasimomenta are beginning to split. When this occurs there is always a degeneracy between the quasimomenta as to which one goes up and which one goes down (this degeneracy is of no physical consequence, it is merely a mathematical hurdle). The numerical fluctuations of the values of the quasimomenta are usually somewhere close to machine precision, $\approx 10^{-15}$, and are difficult to detect. In order to observe the splitting we found it was necessary to manually alter the initial guess for the quasimomenta at these points, forcing one to go up and one to go down [again see Figs. 1(b) and 1(e)].

There is no fundamental limit to the excited states we can reach with this procedure, and similar graphs can be produced for up to approximately $N=20$ particles [see Figs. 2 and 3 as examples of the $(N=20)$-particle gas]. In principle this work could be extended to larger numbers of particles, and in fact we have found the ground state for up to $N \approx 50$. However, the bifurcations in the excited states require some time to locate and we have had to deal with them

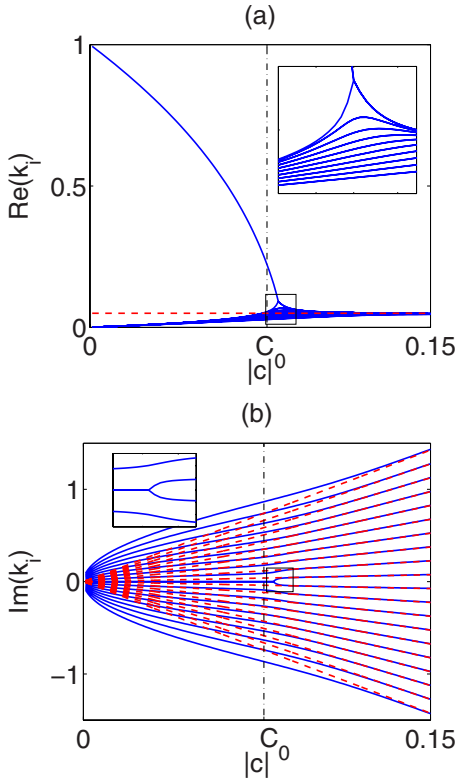

FIG. 2. (Color online) Quasimomenta of the first excited state for $N=20$ particles as a function of the interaction strength c. (a) and (b) show the real and imaginary parts, respectively, of the quasimomenta. The (blue) solid lines are the roots calculated using the Bethe ansatz, whereas the (red) dashed lines show the string solutions given by Eqs. (13), which give the asymptotic behavior of the quasimomenta in the attractive limit. The two solutions are in good agreement above the critical interaction strength, validating the essential properties of the bound states described in Refs. [12,27,50–52]. The inset shows the region where the quasimomenta bifurcate, causing numerical difficulties.

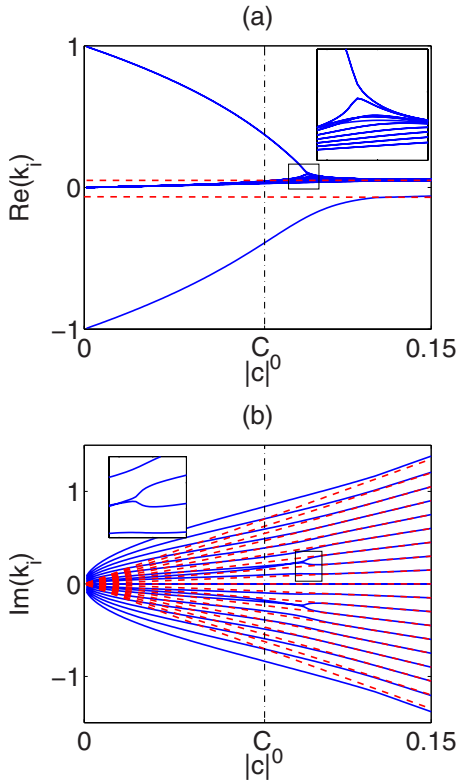

FIG. 3. (Color online) Quasimomenta of one of the second excited states for $N=20$ particles as a function of the interaction strengnth c. (a) and (b) show the real and imaginary parts, respectively, of the quasimomenta. The (blue) solid lines are the roots calculated using the Bethe ansatz, whereas the (red) dashed lines show the string solutions given by Eqs. (16) with $M=1$. The inset shows where the quasimomenta bifurcate for this case.

manually. This means that the algorithm begins to take a considerable amount of time for N significantly larger than 20.

Roots of Eq. (8) for $c<0$ have a far more complicated behavior than in the more commonly studied repulsive regime. Apart from the obvious reason that the quasimomenta can be complex (as opposed to strictly real for the repulsive gas [45]), there also exists the change in behavior at the critical interaction strength C_0. For some time it has been suspected that the roots for large enough attraction would take values on strings in the complex plane which correspond to some bound state of the system [50–52]. That is, the wave function would represent some kind of localized state [12,50] such as

$$\psi_{bound}(\theta_1, \ldots, \theta_N) = \exp\left(-\frac{1}{2}|c|\sum_{\langle i,j\rangle}|\theta_i - \theta_j|\right), \qquad (12)$$

and the corresponding quasimomenta of this state would be

$$k_1 = \frac{K}{N} + \frac{1}{2}(N-1)ic,$$

$$k_2 = \frac{K}{N} + \frac{1}{2}(N-3)ic,$$

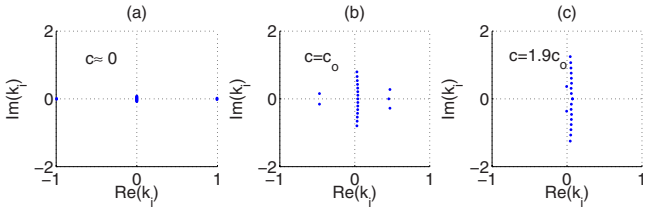

FIG. 4. (Color online) Quasimomenta distribution for $N=20$ particles in the complex plane for different values of interaction strength c for the excited state with quasimomenta distribution $\{-1,-1,0,\ldots,0,1,1,1\}$ at $c=0$. (a) $|c|=10^{-6}$. The quasimomenta are close to the single-particle momenta for the ideal gas. (b) $|c|=C_0\approx 0.079$. Near the mean-field critical point there exists a two-particle bound state, a three-particle bound state, and a 15-particle bound state. (c) $|c|=1.9$. The interaction strength is well past the critical point and the three-particle bound state has collapsed in with the 15-particle bound state; however, there is still a two-particle bound state.

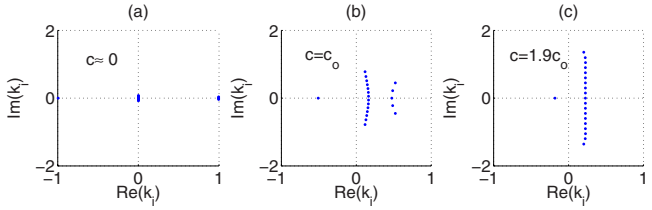

FIG. 5. (Color online) Quasimomenta distribution for $N=20$ particles in the complex plane for different values of interaction strength c for the excited state with quasimomenta distribution $\{-1,0,\ldots,0,1,1,1,1,1\}$. (a) $|c|=10^{-6}$. The quasimomenta are close to the single-particle momenta for the ideal gas. (b) $|c|=C_0 \approx 0.079$. Near the mean-field critical point, there exists a free particle, a five-particle bound state, and a14-particle bound state. (c) $|c|=1.9$. The interaction strength is well past the critical point and the five-particle bound state has combined with the 14-particle bound state, leaving a single free particle.

$$\vdots$$

$$k_N = \frac{K}{N} - \frac{1}{2}(N-1)ic, \tag{13}$$

where $K=\Sigma k_i$ is the total momentum of the state. It is worthwhile to note that, although we refer to the wave function in Eq. (12) as a *localized state* it is not localized to any specific point. Rather it has a localized pair correlation [47]

$$g^{(2)}(\theta,\theta') = \frac{\langle \hat{\Psi}^\dagger(\theta)\hat{\Psi}^\dagger(\theta')\hat{\Psi}(\theta)\hat{\Psi}(\theta')\rangle}{\langle \hat{\Psi}^\dagger(\theta)\hat{\Psi}(\theta)\rangle\langle \hat{\Psi}^\dagger(\theta')\hat{\Psi}(\theta')\rangle}, \tag{14}$$

where $\hat{\Psi}(\theta)$ $[\hat{\Psi}^\dagger(\theta)]$ are bosonic field operators which annihilate (create) a particle at position θ. Thus measurements of the density of an ensemble will always yield a localized projection, while the system is not localized prior to the measurement. One can think of the system prior to the measurement as being in a (macroscopic) superposition of localization at every point on the ring. This form for the quasimomenta given by Eqs. (13) is commonly referred to in the literature as a *string* solution [50–52]. It is often assumed that multiple strings may exist for one system ([50] and references therein), with each string corresponding to a soliton of different momentum. This choice of quasimomenta also seems intuitively reasonable and gives the result, mandated by McGuire [12,50] for the total energy of the bound state,

$$E_K = \frac{1}{N}K^2 - \frac{N(N^2-1)}{12}c^2. \tag{15}$$

The degree to which the system is localized by these string solutions can be quantified by the absolute values of the imaginary parts of the quasimomenta. Thus, in Eqs. (13), as $|c|$ increases, so does the degree of localization (as one would naively expect). However, it is easy to show that in the ideal limit, $c\to 0$, the quasimomenta are exactly the single-particle momentum states. Thus if one accepts the quasimomenta given by Eqs. (13), then one is left with chronic discontinuities in the behavior of the quasimomenta as a function of $|c|$.

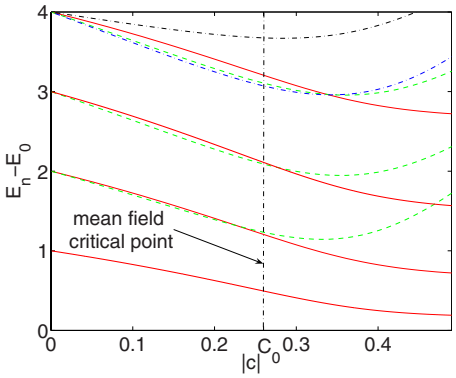

FIG. 6. (Color online) Excitation spectrum of an $(N=6)$-particle system obtained via the Bethe ansatz. The solid (red) lines show the formation of a single bound state. The (green) dashed lines show the formation of two bound states. The (blue) dot-dashed lines show the formation of three separate bound states. The qualitative change in the behavior of the eigenstates at the phase transition point becomes more visible than for the two-particle case (see Fig. 9).

Our results give direct evidence that the two limits are bridged via Eqs. (8). We also find other families of excited states, with multiple bound states forming in the limit of strong attraction. These show agreement with the truncated diagonalization results discussed later in Sec. III C. These families of excited states can be interpreted as the formation of multiple bound states. It is very interesting to observe this intermediate behavior between the ideal gas and strongly attractive gas since this is where soliton formation occurs at zero temperature.

In Fig. 1 we see the behavior of the quasimomenta for a system of $N=6$ particles in the eight lowest-energy states ordered via their energies at $c=0$. As $|c|$ becomes larger, energy level crossings are observed as in Fig. 6. The quasimomenta begin at $c=0$ at their respective single-particle momentum states, and as c becomes more negative the quasimomenta tend toward a string solution as predicted. The initial behavior of the imaginary part of the quasimomenta varies as $\sqrt{|c|}$ for $|c|<C_0$, but for $|c|>C_0$ when the system is in a localized state the low-lying eigenstates have quasimomenta corresponding to the string solutions Eqs. (13).

This is verified again for the $(N=20)$-particle gas in Fig. 2 where the solid blue lines show the quasimomenta as a function of $|c|$ and the red dashed lines show the string solution Eqs. (13), and both are in agreement in the strongly attractive limit. However, we also find excited states that do not agree with Eqs. (13), but instead form multiple bound states. This results in a decrease in the degree of localization. In these cases we find the behavior of the quasimomenta at large $|c|$ to be given by

$$k_1 = \frac{K}{M} + \frac{1}{2}(M-1)ic,$$

$$\vdots$$

$$k_M = \frac{K}{M} - \frac{1}{2}(M-1)ic,$$

$$k_{M+1} = \frac{K'}{N-M} + \frac{1}{2}(N-M-1)ic,$$

$$\vdots$$

$$k_N = \frac{K'}{N-M} - \frac{1}{2}(N-M-1)ic. \tag{16}$$

We interpret this solution physically as an M-particle bound state with momentum K and an $(N-M)$-particle bound state with momentum K'.

Evidence of these states can be seen in Fig. 3 where the solid blue lines show the quasimomenta as a function of $|c|$, whereas the red dashed lines show the solutions given by Eqs. (16) with $M=1$, $K=-1/20$, and $K'=21/380$. In Figs. 1(d) and 1(f) the same kind of behavior is seen for the $(N=6)$-particle gas. The behavior is perhaps clearer in Figs. 4(c) and 5(c), where one can see the two distinct strings in the complex plane. One can derive a simple expression for the energy of these states [similar to Eq. (15)],

$$E^{(1)}_{KK'} = \frac{(N-M)K^2 + MK'^2}{M(N-M)} - \frac{N(N^2-3NM+3M^2-1)}{12}c^2. \tag{17}$$

This trend continues such that three or more bound states of atoms occur within the system. The evidence for this is most easily seen by the grouping of the quasimomenta in the complex plane [Figs. 4(c) and 5(c)].

Thus for this system, once $c<C_0$ and localization has occurred, we observe several different families of solutions. The first is the ground state of the system, corresponding to a single, stationary N-particle soliton. Then there are the elementary excitations of this state whereby the soliton has some (integer valued) total momentum about the ring. Furthermore, there exist the higher-order excitations in which multiple solitons form around the ring. Equally, these multiple solitons can have elementary excitations of their own, corresponding to some integer valued total momentum.

B. Excitation spectrum

We can now calculate the excited states of the system via the Bethe ansatz, using Eq. (9) and the numerically determined roots of Eqs. (8) (the quasimomenta). We show a comparison between the truncated diagonalization approach of Kanamoto *et al.* [23,24] in Sec. III C (see Figs. 9 and 10). We plot the excitation spectrum for $N=6$ particles in Fig. 6 and $N=20$ particles in Fig. 7. The point at which mean-field theory predicts the quantum phase transition, C_0 (see Appendix B), is indicated on all figures with a vertical dot-dashed line. We observe the *sharpening* of the crossover regime as N increases, as expected for a phase transition in the limit of large N. For comparison, the result of a Bogoliubov analysis in the limit of $N\to\infty$ is shown in Fig. 8, which is already in fair agreement with Fig. 7 for only $N=20$ particles. For further details of the mean-field results for this system we refer the reader to Refs. [20,21].

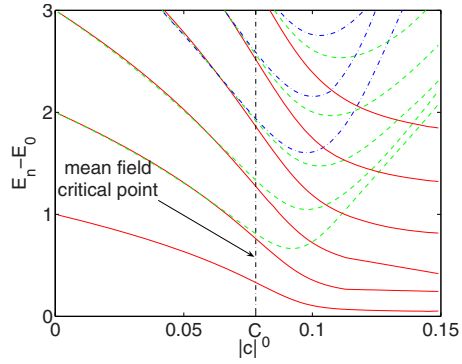

FIG. 7. (Color online) Excitation spectrum of an $(N=20)$-particle system obtained via the Bethe ansatz. The solid (red) lines show the formation of a single bound state. The (green) dashed lines show the formation of two bound states. The (blue) dot-dashed lines show the formation of three separate bound states.

Once the size of the system gets up to around $N=20$, the difference in the behavior of the states for $|c|<C_0$ and $|c|>C_0$ is clear. For the $|c|>C_0$ transition (once the bound state has formed), the different families of solutions to the Bethe ansatz Eqs. (8) (discussed in the previous section) become distinguishable through their separation from the ground state. The solid red lines in Figs. 6 and 7 show the behavior of the single bound states found by McGuire and others [12,27,51,52] given by Eqs. (13), and the green dashed lines show the family of solutions given by Eqs. (16) which are made up of two separate bound states. Finally, the blue dot-dashed lines show the existence of three separate bound states within the gas.

C. Comparison to the truncated Hilbert space diagonalization

The excitation spectrum of the attractive gas has been numerically studied via truncation of the Hilbert space in previous work [23,24]. The key element in the approach is to

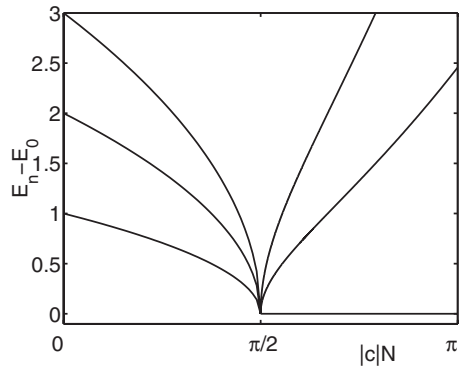

FIG. 8. Bogoliubov excitation spectrum of the 1D Bose gas on a ring with attractive interations. The comparison with Fig. 7 shows reasonable quantitative agreement to the left of the critical point for only $N=20$ particles. To the right of the critical point, there is qualitative agreement through the emergence of a Goldstone mode as well as higher-order branches of excitation.

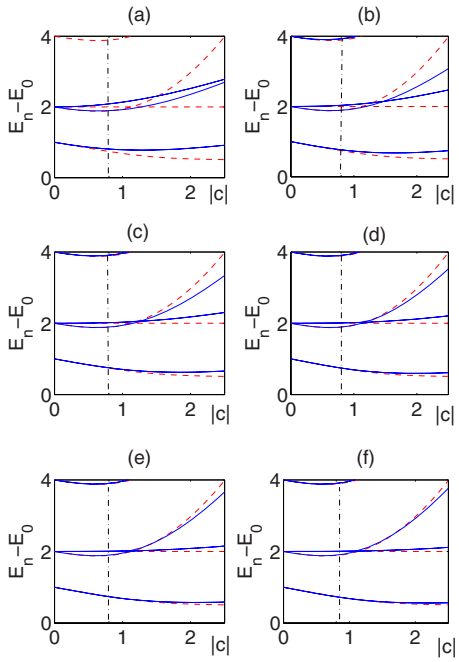

FIG. 9. (Color online) Comparison of the excitation spectrum found via the Bethe ansatz Eqs. (8) [(red) dashed lines] to that found via diagonalization of the truncated Hamiltonian [solid (blue) lines] for an $(N=2)$-particle system. The vertical dash-dotted line marks the meanfield crititical interaction strength C_0 derived in Appendix B. Single-particle momentum state cutoff of (a) ±1, (b) ±2, and so on, up to (f), which has a singleparticle momentum cutoff of ±6.

exclude all single-particle momentum states beyond a particular threshold. The results of these calculations are of course exact at zero interactions, but deviate from the exact solution as the interaction strength $|c|$ is increased. The degree of deviation can of course be decreased by increasing the threshold momentum state; however, the dimension of the Hilbert space will eventually become unmanageably large in doing so. An example of this process is shown in Fig. 9 for a two-particle system, where it is possible to make the cutoff relatively high without having the Hilbert space dimension grow beyond a practical number. The results indicate a good qualitative description from a very small number of momentum states [23]. For example, if $N=200$, a momentum cutoff of ±1 is reasonable up to and even beyond $(c \approx 2c_0)$ the critical point. This was supported by calculations made by Kavoulakis [20], who used a mean-field approximation with a suitably chosen wave function to examine the ground state and low-lying states near the phase transition.

The truncated diagonalization procedure we use follows that of Kanamoto *et al.* [24]. The first quantized Hamiltonian in Eq. (1) is rewritten in second quantized formalism as

$$\hat{H} = \int_0^{2\pi} d\theta \left(-\hat{\Psi}^\dagger(\theta) \frac{\partial^2}{\partial \theta^2} \hat{\Psi}(\theta) + c\hat{\Psi}^{\dagger 2}(\theta)\hat{\Psi}^2(\theta) \right), \quad (18)$$

where $\hat{\Psi}(\theta)$ is the bosonic field operator that annihilates a boson at coordinate θ and obeys the usual commutation rules

TABLE I. The size of the Hilbert space and subspaces for selected particle numbers and momentum cutoffs. This gives an idea of the size of computation required for the truncated diagonalization procedure.

N	m	Hilbert space dimension	Number of subspaces	Dimension of largest subspace
2	3	6	5	2
	5	15	9	3
	7	28	13	4
20	3	231	41	11
	5	10626	81	318
	7	230230	121	5444
200	3	20301	401	101
	5	70058751	801	230673

and the periodic boundary conditions of the ring geometry. This field operator is then approximated by its truncated expansion in terms of single-particle states

$$\hat{\Psi}(\theta) = \sum_{j=-k_0}^{k_0} \varphi_j(\theta)\hat{c}_j, \quad (19)$$

where $\varphi_j(\theta)$ is the single-particle eigenstate with angular momentum j (see Appendix A), $\hat{c}_j$ annihilates a boson with angular momentum j, and k_0 is the single-particle momentum state cutoff. In this manner, for finite N and finite k_0, $\hat{H}$ is a finite matrix. Furthermore, $\hat{H}$ (when written in the appropriately ordered basis set) will be block diagonal, as it can be divided into total momentum subspaces that can be individually diagonalized. If we use m to denote the total number of single-particle momentum states used in the expansion (i.e., $m=2k_0+1$) then the total dimension of the Hilbert space will be the binomial coefficient $\binom{N+m-1}{N}$. This Hilbert space will split up into $N(m-1)+1$ (total momentum) subspaces. The largest subspace will be the zero-momentum subspace. For example, if we were to consider a gas of $N=20$ particles with the momentum cutoff at ±2 $(m=5)$, then the total dimension of the truncated Hilbert space would be 10 626. However, this splits up into 81 different total momentum subspaces, the largest of which has dimension 318, which can be exactly diagonalised on a standard desktop PC. Table I gives an indication of the scale of computation required for the truncated diagonalization procedure.

In Fig. 10 we show a comparison between excitation spectra obtained from the truncated diagonalization procedure and the Bethe ansatz for the $(N=20)$-particle gas. We observe that for $m=3$ (single-particle momentum cutoff at ±1) the truncated diagonalization overestimates the energy difference between ground and excited states in the crossover regime, but underestimates the difference in the regime where the bound states have formed. For $m=5$ (single-particle momentum cutoff at ±2) the agreement between the two methods in the crossover regime is vastly improved; however, the truncated diagonalization still underestimates

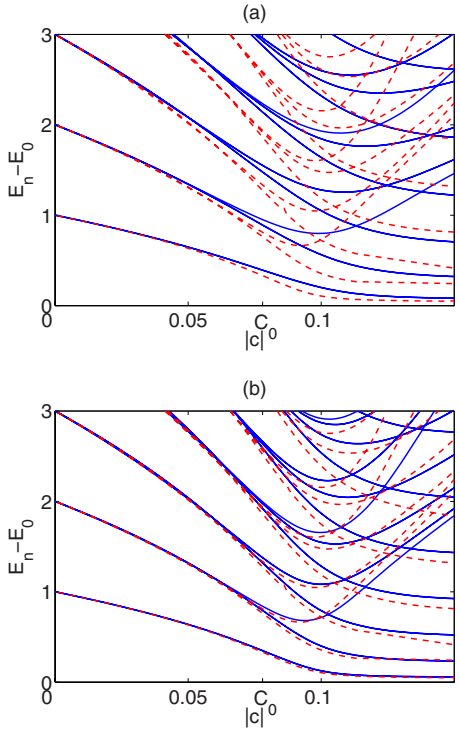

FIG. 10. (Color online) Comparison of the excitation spectrum found via the Bethe ansatz Eqs. (8) [(red) dashed lines] to that found via diagonalization of the truncated Hamiltonian [solid (blue) lines] for an ($N=20$)-particle system. (a) Truncation at $m=3$ (single-particle momentum states $0, \pm 1$). (b) Truncation at $m=5$ (single-particle momentum states $0, \pm 1, \pm 2$).

the difference between ground and excited states in the bound state regime.

IV. REPULSIVE GAS: $c > 0$

The root-finding algorithm can easily be applied to the case of repulsive attractions. A proof exists showing that all roots of Eqs. (8) lie on the real axis [45]. This means that we avoid the problems associated with the bifurcations that appeared in the attractive case, and the situation is therefore significantly easier. In this case the limiting behavior as $c \to \infty$ of the quasimomenta is given by the single-particle momentum states of an ideal Fermi gas [11,53]. This limit is known as the Tonks-Girardeau gas and has been experimentally observed [3].

In this work, we use our numerical root-finding algorithm to bridge from the ideal gas to the Tonks-Girardeau gas. We do so for both the ground state and the low-lying excited states for finite numbers of particles. The ground state has appeared previously in the work of Sakmann *et al.* [25]. The thermodynamic limit has been addressed in the homogeneous case [43,44,54] and the trapped case [55] (and references therein).

A. Quasimomenta

The root-finding algorithm is essentially unchanged from the case of attractive interactions. It is worth mentioning, however, that, since there is no phase transition in the repulsive gas, the step size Δc can be increased without sacrificing a reasonable initial guess. In our calculations we use $\Delta c = 10^{-4}$ for $0 \leq c \leq 1$, then $\Delta c = 1$ $\Delta c = 10^{-3}$ for $1 \leq c \leq 6$, then $\Delta c = 10^{-2}$ for $6 \leq c \leq 20$, then $\Delta c = 10^{-1}$ for $20 \leq c \leq 100$, and finally for $c \geq 100$.

In Fig. 11 we see how the quasimomenta behave as a function of the interaction strength c. The single particle excitations of *bosons* with $c=0$ result in single-particle excitations of the ideal *fermions* at $c=\infty$. The concept of particle-hole excitations for the strongly repulsive gas (see Refs. [44,50]) is clear in Fig. 11. We see that low-lying excited state quasimomenta are similar to those for the ground state, but with a small number of quasimomenta excited, leaving behind *holes*.

It is possible to push the algorithm for the repulsive case to much higher atom numbers than with the attractive case. This is due to the absence of the exotic features in the quasimomenta spectrum (see, for example, the splitting occurring in the insets of Figs. 2 and 3). In Fig. 12 we show the ground state quasimomenta for a repulsive gas with $N=50$.

B. Excitation spectrum

As for the attractive gas, the excitation spectrum can be found using Eq. (9). In Fig. 13 we show the energies of the low-lying excited states for $c > 0$. The red dashed lines show the result obtained from truncating the Hilbert space down to five single-particle states and diagonalizing the Hamiltonian (see Sec. III C). The truncation procedure is accurate for small enough values of c (see the inset of Fig. 13 where c runs from zero to one), but fails as c increases beyond one. The dotted line shows the ground state energy of an ($N=20$)-particle Fermi gas.

V. CONCLUSIONS

We have studied the behavior of the roots of the Bethe ansatz Eqs. (8) for the 1D Bose gas on a ring as a function of the interaction strength for both the attractive case (up to $N=20$ particles) and the repulsive case. We used these roots to determine the exact many-body energy spectrum of the one-dimensional Bose gas with δ-function interactions in a 1D ring trap for small numbers of particles. We compared our results to those obtained via the approximate method of truncated diagonalization, to which we found good qualitative agreement and reasonable quantitative agreement for small enough interaction strength. We have quantitatively addressed the issue of when it is reasonable to assume a bound state solution to Eqs. (8), and have quantified the deviations from the string solutions that occur for a finite-density gas, thus establishing the point at which the string solutions become valid. Furthermore, we found evidence for the existence of multiple, independent *solitons* existing on the ring. These excitations had been hypothesized in previous work; however, to the best of our knowledge this is the first direct evidence of their existence. We have described the analytical expressions for the quasimomenta of these families of string

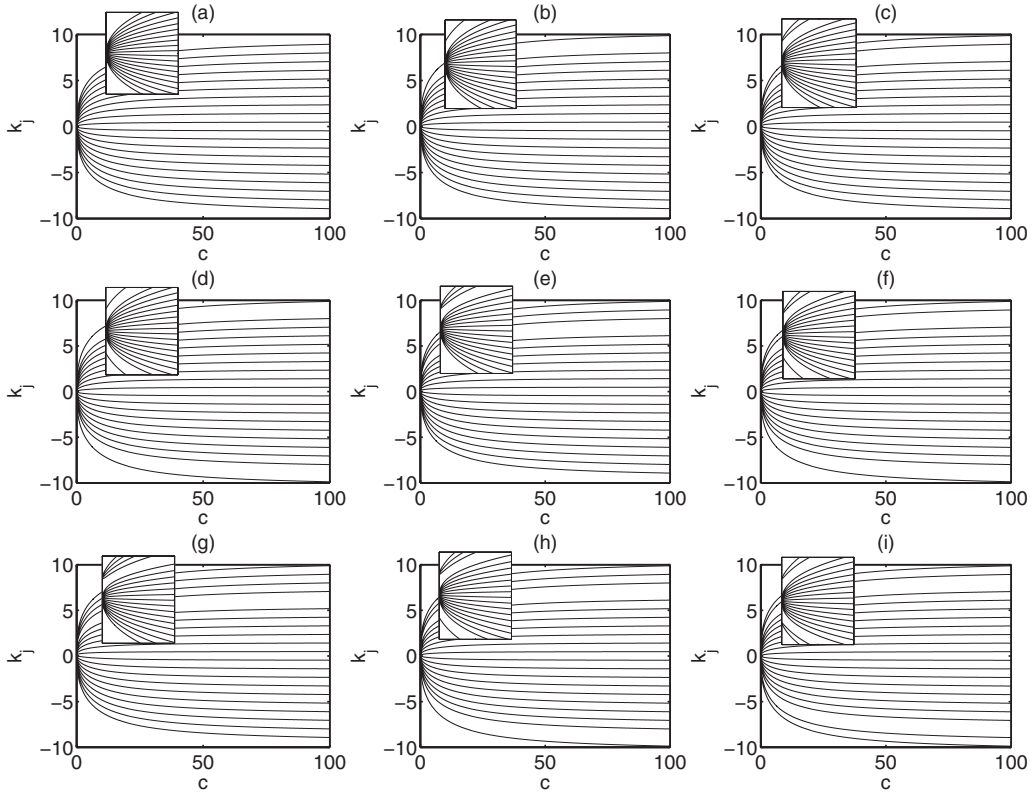

FIG. 11. Quasimomenta as a function of interaction strength for $c>0$. (a) Ground state of the ideal Bose gas. (b) First excited state of the ideal Bose gas (degenerate with the state $k_j \to -k_j$). (c),(d) Degenerate second excited states of the ideal Bose gas (also degenerate with the state $k_j \to -k_j$). (e),(f) Degenerate third excited states of the ideal Bose gas (also degenerate with the state $k_j \to -k_j$). (g),(h),(i) Degenerate fourth excited states of the ideal Bose gas (also degenerate with the state $k_j \to -k_j$). The insets in (a)–(i) show the behavior close to $c=0$.

solutions in Eqs. (16) and an expression for the energies of these states.

It may be interesting in the future to make use of the solutions found in this paper to calculate correlation functions for the one-dimensional Bose gas. In general this is a nontrivial task, as quantities such as $g^{(m)}$ [defined similarly as $g^{(2)}$ in Eq. (14), but now as a product of m creation and m annihilation operators], when written in first quantization involve integrals over the product $\psi^*\psi$. Therefore if one proceeds naively the computational complexity scales as $(N!)^2$. One therefore requires a more advanced approach to this problem [47,56].

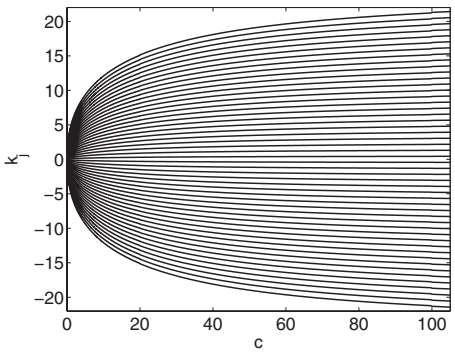

FIG. 12. Quasimomenta as a function of interaction strength for an $(N=50)$-particle repulsive gas.

ACKNOWLEDGMENTS

This work was supported by the Australian Research Council Centre of Excellence for Quantum-Atom Optics and the Queensland State government. The authors wish to acknowledge the useful discussions with all members of the

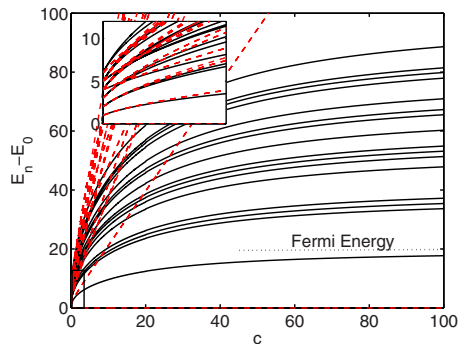

FIG. 13. (Color online) Excitation spectrum of an $(N=20)$-particle gas with repulsive interactions $c>0$ [solid (black) lines]. The (red) dashed lines were obtained by truncating the Hilbert space down to five single-particle momentum states. The inset shows the region of $0<c<1$ where the truncated diagonalization is accurate. The dotted lines shows the ground state energy of a free Fermi gas, and the so-called Tonks Girardeau ground state asymptotes to this value.

University of Queensland node. A.G.S. wishes to thank particularly C. Foster and D. Barry for technical help with computational tasks and J. S. Caux and N. Oelkers for useful discussions.

APPENDIX A: SINGLE PARTICLE IN A RING

The single-particle Hamiltonian is

$$-\frac{\hbar^2}{2mR^2}\frac{\partial^2}{\partial\theta^2}\varphi(\theta)=E\varphi(\theta), \tag{A1}$$

and the single-particle energy eigenvalues are

$$E_k=\frac{k^2\hbar^2}{2mR^2}, \quad k=0,\pm 1,\pm 2\ldots, \tag{A2}$$

with corresponding eigenstates

$$\varphi_k(\theta)=\frac{1}{\sqrt{2\pi}}e^{ik\theta}. \tag{A3}$$

APPENDIX B: THE MEAN-FIELD CRITICAL POINT

We include a derivation of the mean-field critical point of localization using the same approach as Kavoulakis [20]. Considering the Hamiltonian (18) we define a mean field $\psi(\theta)$ and approximate the system as having the many-body wave function $\Pi_i\psi(\theta_i)$. We next expand $\psi(\theta)$ in terms of single-particle states given by Eqs. (A3); however, we truncate all momentum states greater than 1,

$$\psi(\theta)=\alpha_{-1}\varphi_{-1}(\theta)+\alpha_0\varphi_0(\theta)+\alpha_1\varphi_1(\theta). \tag{B1}$$

We then assume $|\alpha_0|\gg|\alpha_{-1}|,|\alpha_1|$ and use the symmetry $|\alpha_{-1}|=|\alpha_1|$ and finally the normalization condition $|\alpha_{-1}|^2+|\alpha_0|^2+|\alpha_1|^2=1$. The energy per particle ϵ is then found to be

$$\epsilon=2|\alpha_1|^2+\frac{\gamma}{2}[|\alpha_0|^4+|\alpha_{-1}|^4+|\alpha_1^4|+4|\alpha_0|^2|\alpha_{-1}|^2 + 4|\alpha_0|^2|\alpha_1|^2+4|\alpha_{-1}|^2|\alpha_1|^2+2\alpha_0^2\alpha_{-1}^*\alpha_1^*+2(\alpha_0^2)^*\alpha_{-1}\alpha_1], \tag{B2}$$

where $\gamma=Nc/\pi$. Setting $\alpha_j=|\alpha_j|e^{i\phi_j}$, then ϵ is minimized by choosing $\phi_{-1}+\phi_1-2\phi_0=0$, and the normalization condition further simplifies Eq. (B2) to

$$\epsilon-\frac{\gamma}{2}=2|\alpha_1|^2(1+2\gamma)-7\gamma|\alpha_1|^4. \tag{B3}$$

From Eq. (B3) it is straightforward to see that the approach one must take in order to minimize ϵ will depend on whether $-1/2<\gamma<0$ (in which case the gas is delocalized) or $\gamma<-1/2$ (in which case the gas is localized). Thus there exists a critical interaction strength of

$$C_0=\frac{\pi}{2N}. \tag{B4}$$

[1] A. Gorlitz *et al.*, Phys. Rev. Lett. **87**, 130402 (2001).
[2] B. Laburthe Tolra, K. M. O'hara, J. H. Huckans, W. D. Phillips, S. L. Rolston, and J. V. Porto, Phys. Rev. Lett. **92**, 190401 (2004).
[3] T. Kinoshita, T. Wenger, and D. S. Weiss, Science **305**, 1125 (2004).
[4] T. P. Meyrath, F. Schreck, J. L. Hanssen, C. S. Chu, and M. G. Raizen, Phys. Rev. A **71**, 041604(R) (2005).
[5] Z. Hadzibabic, S. Stock, B. Battelier, V. Bretin, and J. Dalibard, Phys. Rev. Lett. **93**, 180403 (2004).
[6] N. L. Smith *et al.*, J. Phys. B **38**, 223 (2005).
[7] S. Burger, F. S. Cataliotti, C. Fort, F. Minardi, M. Inguscio, M. L. Chiofalo, and M. P. Tosi, Phys. Rev. Lett. **86**, 4447 (2001).
[8] M. Greiner *et al.*, Appl. Phys. B: Lasers Opt. **73**, 769 (2001).
[9] F. Schreck, L. Khaykovich, K. L. Corwin, G. Ferrari, T. Bourdel, J. Cubizolles, and C. Salomon, Phys. Rev. Lett. **87**, 080403 (2001).
[10] H. Moritz, T. Stöferle, M. Köhl, and T. Esslinger, Phys. Rev. Lett. **91**, 250402 (2003).
[11] E. H. Lieb and W. Liniger, Phys. Rev. **130**, 1605 (1963).
[12] J. B. McGuire, J. Math. Phys. **5**, 622 (1964).
[13] S. Sachdev, *Quantum Phase Transitions* (Cambridge University Press, New York, 1999).
[14] M. Greiner *et al.*, Nature (London) **415**, 39 (2002).
[15] P. D. Drummond, R. M. Shelby, S. R. Friberg, and Y. Yamamoto, Nature (London) **365**, 307 (1993).
[16] S. J. Carter, P. D. Drummond, M. D. Reid, and R. M. Shelby, Phys. Rev. Lett. **58**, 1841 (1987).
[17] K. E. Strecker, G. B. Partridge, A. G. Truscott, and R. G. Hulet, Nature (London) **417**, 150 (2002).
[18] L. Khaykovich *et al.*, Science **296**, 1290 (2002).
[19] S. L. Cornish, S. T. Thompson, and C. E. Wieman, Phys. Rev. Lett. **96**, 170401 (2006).
[20] G. M. Kavoulakis, Phys. Rev. A **67**, 011601(R) (2003).
[21] R. Kanamoto, H. Saito, and M. Ueda, Phys. Rev. A **67**, 013608 (2003).
[22] R. Kanamoto, H. Saito, and M. Ueda, Phys. Rev. A **68**, 043619 (2003).
[23] R. Kanamoto, H. Saito, and M. Ueda, Phys. Rev. A **73**, 033611 (2006).
[24] R. Kanamoto, H. Saito, and M. Ueda, Phys. Rev. Lett. **94**, 090404 (2005).
[25] K. Sakmann, A. I. Streltsov, O. E. Alon, and L. S. Cederbaum, Phys. Rev. A **72**, 033613 (2005).
[26] L. Salasnich, J. Phys. B **39**, 1743 (2006).
[27] F. Calogero and A. Degasperis, Phys. Rev. A **11**, 265 (1975).
[28] N. Oelkers and J. Links, Phys. Rev. B **75**, 115119 (2007).
[29] A. Seel, T. Bhattacharyya, F. Göhmann, and A. Klümper, J. Stat. Mech.: Theory Exp. (2007) P08030.
[30] L. Amico and V. Korepin, Ann. Phys. (N.Y.) **314**, 496 (2004).
[31] A. Kundu and O. Ragnisco, J. Phys. A **27**, 6335 (1994).
[32] M. Olshanii, Phys. Rev. Lett. **81**, 938 (1998).
[33] A. Parola, L. Salasnich, R. Rota, and L. Reatto, Phys. Rev. A **72**, 063612 (2005).

[34] L. Salasnich, A. Parola, and L. Reatto, Phys. Rev. A **70**, 013606 (2004).
[35] E. M. Wright, J. Arlt, and K. Dholakia, Phys. Rev. A **63**, 013608 (2000).
[36] S. Gupta, K. W. Murch, K. L. Moore, T. P. Purdy, and D. M. Stamper-Kurn, Phys. Rev. Lett. **95**, 143201 (2005).
[37] A. S. Arnold, C. S. Garvie, and E. Riis, Phys. Rev. A **73**, 041606(R) (2006).
[38] O. Morizot, Y. Colombe, V. Lorent, H. Perrin, and B. M. Garraway, Phys. Rev. A **74**, 023617 (2006).
[39] I. Waki, S. Kassner, G. Birkl, and H. Walther, Phys. Rev. Lett. **68**, 2007 (1992).
[40] E. Courtade, O. Houde, J. F. Clement, P. Verkerk, and D. Hennequin, Phys. Rev. A **74**, 031403(R) (2006).
[41] H. Bethe, Z. Phys. **71**, 205 (1931).
[42] J. G. Muga and R. F. Snider, Phys. Rev. A **57**, 3317 (1998).
[43] C. N. Yang, Phys. Rev. Lett. **19**, 1312 (1967).
[44] C. N. Yang and C. P. Yang, J. Math. Phys. **10**, 1115 (1969).
[45] V. E. Korepin, N. M. Bogoliubov, and A. G. Izergin, *Quantum Inverse Scattering Method and Correlation Functions* (Cambridge University Press, New York, 1993).
[46] M. Takahashi, *Thermodynamics of One-Dimensional Solvable Models* (Cambridge University Press, New York, 2005).
[47] P. Calabrese and J.-S. Caux, Phys. Rev. Lett. **98**, 150403 (2007).
[48] J.-S. Caux and P. Calabrese, Phys. Rev. A **74**, 031605(R) (2006).
[49] It is necessary to use small random numbers to keep the quasimomenta distinct from one another.
[50] H. B. Thacker, Rev. Mod. Phys. **53**, 253 (1981).
[51] Y. Castin and C. Herzog, C. R. Acad. Sci., Ser IV: Phys., Astrophys. **2**, 419 (2001).
[52] Y. Lai and H. A. Haus, Phys. Rev. A **40**, 854 (1989).
[53] M. Girardeau, J. Math. Phys. **1**, 516 (1960).
[54] E. H. Lieb, Phys. Rev. **130**, 1616 (1963).
[55] D. S. Petrov, G. V. Shlyapnikov, and J. T. M. Walraven, Phys. Rev. Lett. **85**, 3745 (2000).
[56] A. G. Sykes and M. J. Davis (unpublished).
[57] As an example of a mean-field analysis of the system for $c < c_0$, when the soliton state has formed, see A. Montina and F. T. Arecchi, Phys. Rev. A **71**, 063615 (2005).
[58] Yajiang Hao, Yunbo Zhang, J. Q. Liang, and Shu Chen, Phys. Rev. A **73**, 063617 (2006).